

E-ISSN: 2664-8784 P-ISSN: 2664-8776 Impact Factor: RJIF 8.26 IJRE 2025; 7(2): 110-123 © 2025 IJRE

www.engineeringpaper.net Received: 08-08-2025 Accepted: 11-09-2025

KwangIl Son

Faculty of Electronics, Kim Chaek University of Technology, Pyongyang, Democratic People's Republic of Korea

Nam Chol Yu

Faculty of Electronics, Kim Chaek University of Technology, Pyongyang, Democratic People's Republic of Korea

Design, simulation and fabrication for improving the spectral performance of sunshine sensor by using $Cd_xZn_{1-x}S/CdTe/Cd_xTe$ solar cell with auxiliary absorber layer

KwangIl Son and Nam Chol Yu

DOI: https://www.doi.org/10.33545/26648776.2025.v7.i2b.130

Abstract

Cd_xZn_{1-x}S/CdTe/Cd_xTe solar cell with auxiliary absorber layer was used as sensors with spectral characteristics required for daylight sensing. A simulation of the structure and spectral characteristics of the sensor was performed using the S.TCAD semiconductor device simulation tool to verify the spectral band broadening and determine the optimum thickness of each layer for sensor fabrication. We have analyzed the current-voltage characteristics, spectral response characteristics of the solar cell for sensors and then examined the solar cells using the electroluminescence detection device. The design of the structure and circuit of the sunshine sensor was carried out, finally the characteristics are verified, compared with the CSD3 sensor.

Keywords: Sunshine sensor, solar cell, simulation, auxiliary absorber layer, spectral response

Introduction

The real-time and accurate observation of sunshine time is of great importance in analyzing and predicting solar energy development, meteorological observation, agricultural production, architectural design, environmental conditions, etc ^[1]. Daylight is the time that sunlight is illuminated by the ground, and World Meteorological Organization (WMO) has defined the sum of the times solar radiation intensity exceeds $120 \text{ W/m}^2 \pm 20\%$ ^[2, 3].

Typical sunshine sensors include thermal-electric sensors [3] and photo-electric sensors [1, 2, 4-6]. The solar cell with thermocouples is not affected by temperature, and the measurement accuracy is relatively high, but the response rate is low because it is based on heating during the measurement. As a result, we cannot fully capture the fast fluctuations in radiation caused by partial clouds, and also the fabrication is complex and costly compared to other sensors. On the other hand, the sunshine sensor using light-sensitive elements represent good real-timeness, easy automation and high accuracy.

Currently, for the daylight time measurements, sunshine sensors using photodiodes and photoresistors have been widely used in the world. Optical sensors have the advantages of simple structure, long lifetime, and direct conversion of light into electrical signals. However, the photoresistances are non-linear in the light intensity and current, and there are errors in the measurements [1]. The spectral range of the photodiode-based sensor is 0.4-1.1 um, which is not responsive to a wide solar spectrum. Besides the photodiodes, phototransistors and photoresistors, solar cells have a large chip area and are more efficient and reliable in light conversion than other photosensitive devices. In addition, a solar cell has a linear relationship between currents at light intensities above a certain threshold, long service life, easy fabrication, and low cost. Hence, solar cells are widely used as light sensors.

We have presented a challenge to fabricate solar cells with improved spectral properties using CdS/CdTe solar cells. CdTe has a band gap (Eg) of 1.45 eV, an absorption coefficient of more than 5×10^5 /cm, and is a direct-bandgap semiconductor, which is well suited for solar cell materials. CdTe with a thickness of more than 2 μ m can absorb about 99% of photons with energies greater than the band gap (Eg) ^[7,8]. However, the band gap of CdS and CdTe is 2.45 eV and 1.45 eV, respectively, so it is undesirable that CdS/CdTe solar cells has narrow optical wavelength range of 500-850 nm.

Correspondence KwangIl Son

Faculty of Electronics, Kim Chaek University of Technology, Pyongyang, Democratic People's Republic of Korea

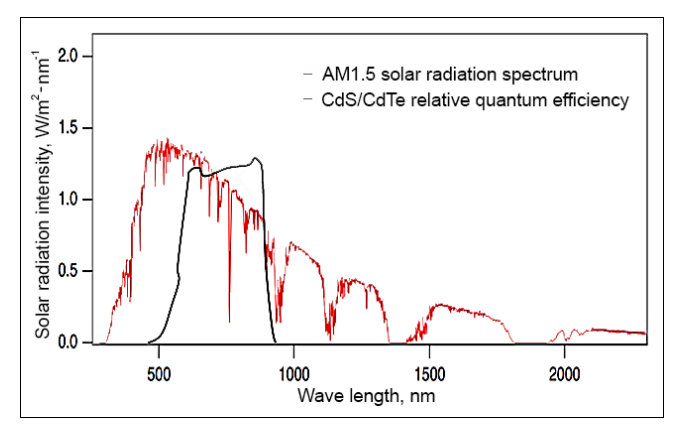


Fig 1: Spectral response characteristics and solar radiation spectrum of CdTe.

As shown in figure 1, the wavelength range of the solar radiation spectrum is 300-3000 nm, and the intensity of the solar spectrum radiation with wavelength is expressed by the following expression [9]:

$$I(\lambda) = 0.06977 + 7.0625 \left(1 - e^{\frac{-(\lambda - 0.26053)}{0.15994}}\right)^{2.28411} e^{\frac{-(\lambda - 0.26053)}{0.15994}} (1)$$

The wavelength range of solar radiation is wide, but most of the energy is concentrated near the wavelength of 0.3-1.2 μ m, which accounts for 99% of the total energy. The wavelength range of CdS/CdTe solar cells is 500-850 nm, which is about 10% of the solar spectrum.

Recently, there is an increasing interest in the study to broaden the spectral response range of CdTe solar cells. First, many attempt have been made to increase the amount of light available for CdTe absorption by using materials with wider band gap than CdS as window layers. Instead of conventional CdS, a wide band gap material such as Cd1-_xZn_xS was used as a window layer to extend the lowerbound transmission wavelength of the solar cell to 400 nm, allowing more light to be transferred to the absorber layer, thus improving the spectral response [10-16]. Next, the study was carried out to extend the light absorption band of the absorber layer [17]. It has been reported that the absorption wavelength of the solar cell was increased by inserting binary Cd_xTe film material for this purpose. The band gap of Te (0.33 eV) is relatively narrow, and when the ratio of Cd to Te is varied from 0 to 1, the band gap of Cd_xTe thin films varies from 0.33 eV to 1.45 eV. By inserting Cd_xTe thin films with tunable band gap, light with the wavelength up to 860 nm, infrared light is absorbed, thereby increasing the photocurrent of the solar cell. It was found that Cd_xTe thin films were intercalated between CdS and CdTe, between CdTe and back electrode to extend the absorption spectral band and improve the back contact. However, the investigation of the composition ratio and films properties were not discussed in detail. In addition, the authors [18] analyzed the structural and optical properties of CdTe2 films

prepared by electrodeposition, and reported that CdTe₂ with bandgap of 1.08 eV can be used as a light absorbing material.

In this paper, we will set up and solve the following problem to fabricate a solar cell using CdTe solar cells. First, we propose a CdTe solar cell with Cd_xTe ($x=0.2\sim0.8$) auxiliary absorber layer, establish a simulation system using a semiconductor device simulation tool (Silvaco TCAD) [19] and determine the appropriate structural parameters. Second, solar cells for sunshine sensor are fabricated and tested by electroluminescence. Third, the design and fabrication of the solar cell and its characterization are carried out to verify its effectiveness.

2. Simulation of spectral characteristics and determination of optimum thickness of solar cells

It is important to extend the absorption wavelength range of incident light for the development of sunshine sensors using CdTe solar cells. We analyzed the spectral characteristics of CdTe solar cells with Cd_{1-x}Zn_xS and Cd_xTe thin films as window and auxiliary absorber layers using SILVCO TCAD simulation software, a semiconductor and integrated circuit simulation system, to determine the optimum thickness of the thin films. The x values for Cd_{1-x}Zn_xS and Cd_xTe were set to 0.9 and 0.2, respectively, through the analysis of the influence of the parameters on the properties of the films. TCAD has been a powerful tool for device experts and designers, with extensive physical models that can accurately describe all the physical phenomena occurring in semiconductor devices and with high numerical capabilities and scientific results processing systems using TONYPLOT [19]

Figures 2 and 3 show the simulation flowchart for the simulation of the structure and characteristics of the solar cell to be simulated.

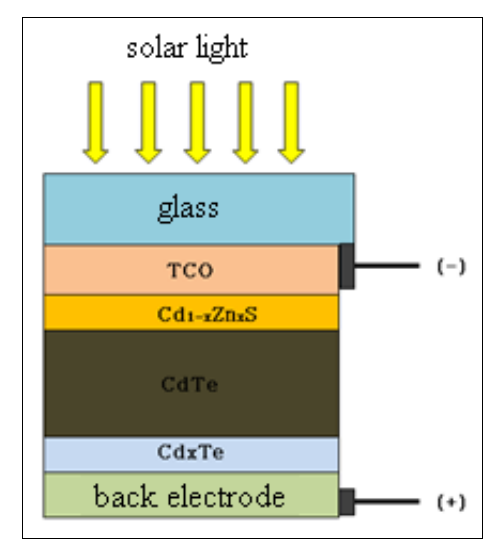


Fig 2: Structure of solar cell for simulation

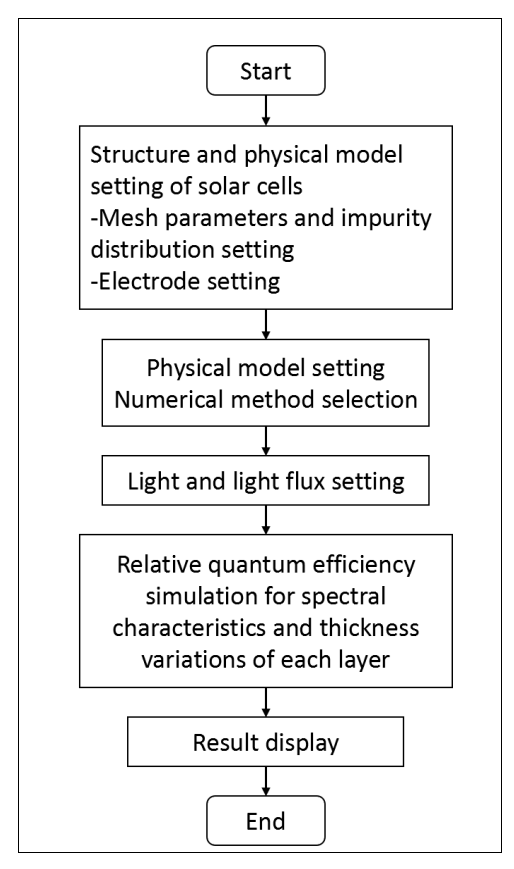
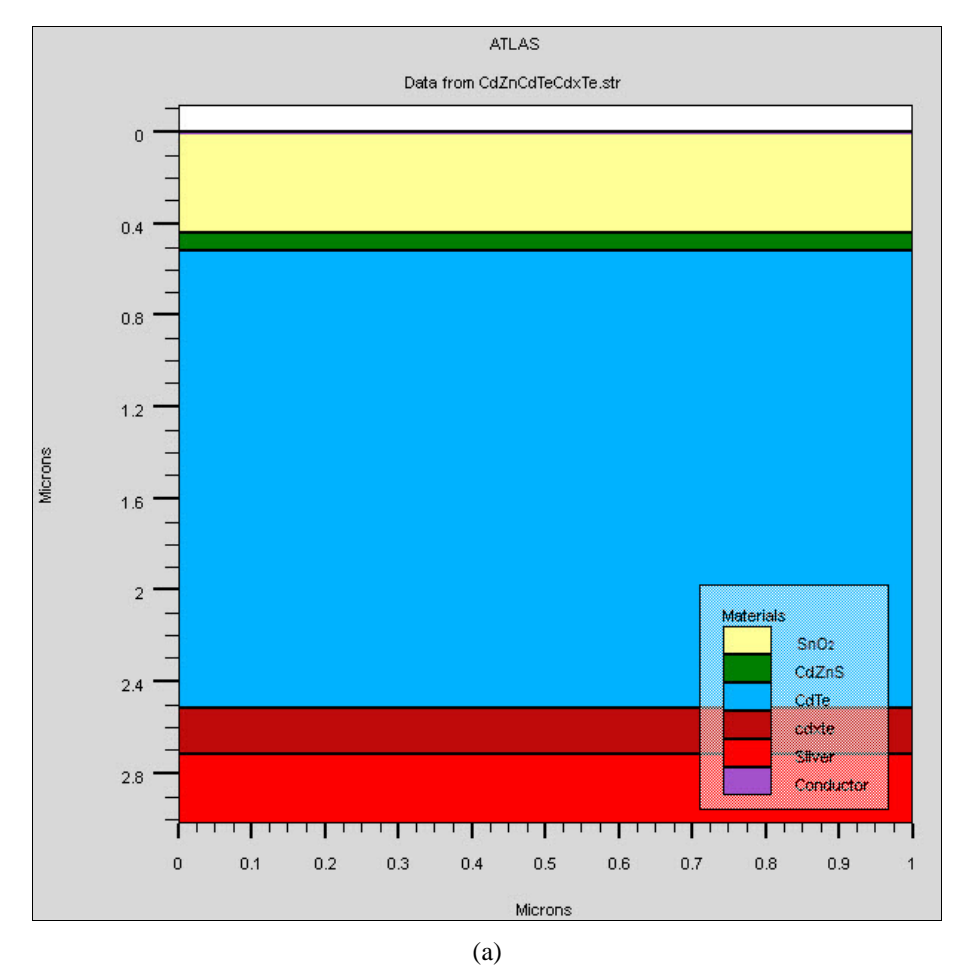


Fig 3: Simulation flow chart

2.1. Simulation structure and physical model setup

Fig. 4 shows the simulated structure and mesh shape of the solar cell.



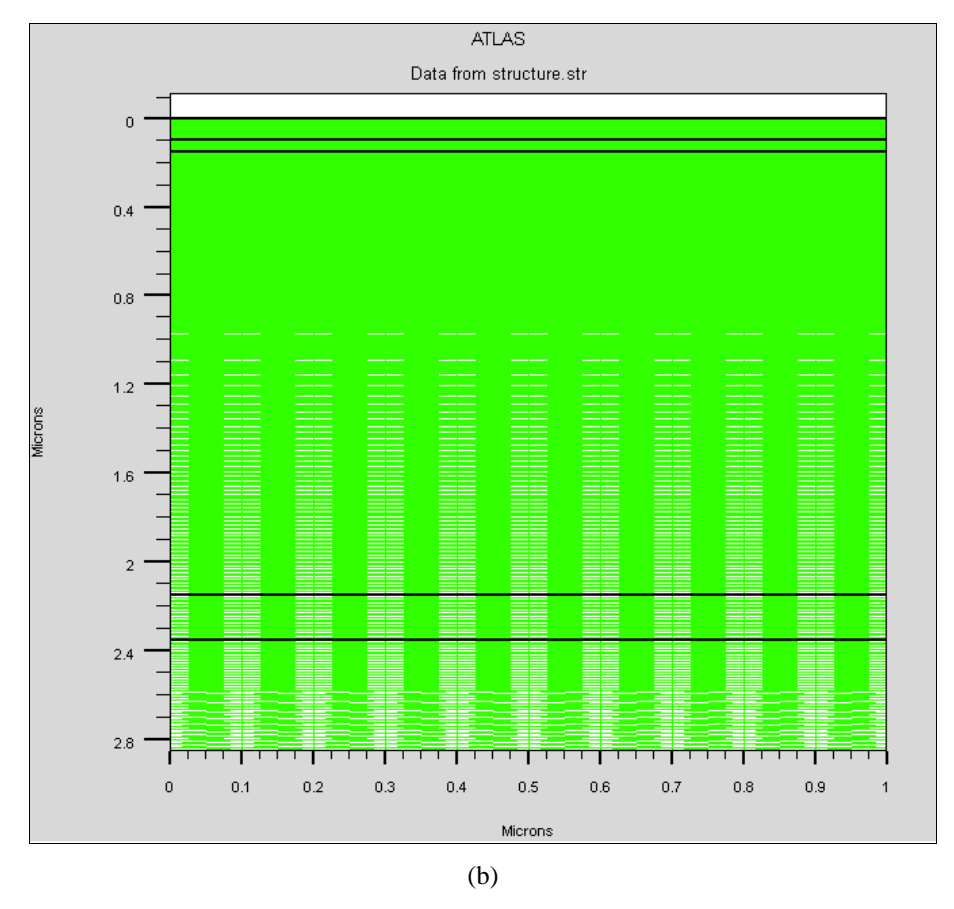


Fig 4: Solar cell simulation structure and mesh segmentation

As shown in Fig. 4a, the CdTe solar cell to be simulated consists of a glass plate, transparent conductive layer, window layer, absorber layer, auxiliary absorber layer and back electrode. For mesh segmentation, the x-axis segmentation interval was set to 0.01 μ min autosegmentation mode and the y-axis was set to 40, 15, 40 and 20, respectively. In the simulations, the material parameters of the transparent conductive layer, window layer, absorber layer and auxiliary absorber layer of the solar cell were used in the literature [16, 17] (Table 1).

Table 1: Material properties parameters used in the simulations

Parameter	SnO ₂	Cd _{0.1} Zn _{0.9} S	CdTe	Cd _{0.2} Te
$W(\mu m)$	0.1	0.02~0.1	0.1~5	0.05-0.3
ϵ/ϵ_0	9.0	9.3	9.4	10
μc(cm/Vs)	100	50	320	115
μp(cm/Vs)	25	7	40	16
E _g (eV)	3.6	3.34	1.45	1.05
Nv(cm ⁻³)	1.8×10 ¹⁹	1.7×10^{19}	1.8×10^{19}	1.8×10^{19}
$N_c(cm^{-3})$	2.2×10^{18}	2.1×10^{18}	7.5×10^{17}	7.5×10^{17}
χ(eV)	4.5	3.94	4.28	4.06

We also used the SRH model (Shockley-Reed-Hall recombination model), as a carrier generation-recombination model for the simulations. The SRH models used in the simulations are as follows [20].

$$R_{SRH} = \frac{pn - n_i^2}{\tau_p[n + n_t] + \tau_n[p + p_t)]} \tag{4}$$

where n_b p_t are the electron and hole densities when the quasi-Fermi level matches the trap level, and τ_p , τ_n are the

generation-recombination lifetimes of holes and electrons. The density of electrons and holes is as following.

$$p_t = N_V exp \frac{E_V - E_t}{k_B T} \tag{5}$$

$$n_t = N_C exp \frac{E_t - E_c}{k_B T} \tag{6}$$

The generation-recombination lifetimes of electrons and holes at room temperature are.

$$\tau_p = \frac{1}{\sigma_p N_t V_{th_p}} \tag{7}$$

$$\tau_n = \frac{1}{\sigma_n N_t V_{th n}} \tag{8}$$

where σ_p , σ_n is the trap cross-section of holes and electrons, N_t is the defect concentration, V_{th_n} , V_{th_p} are the thermal velocity of electrons and holes.

$$V_{th_p} = \sqrt{\frac{3k_BT}{m_{e,h}^*}} \tag{9}$$

2.2. Simulation of spectral characteristics of solar cells

The spectral characteristics of $Cd_{0.1}Zn_{0.9}S/CdTe/Cd_{0.2}Te$ solar cell and the conventional CdS/CdTe solar cell are simulated and compared. The simulated wavelength range was set to 100-1500 nm and the interval to 100 nm. In

S.TCAD, we simulated the light source and spectral characteristics using the following statement. beam num=1 x.orig=0.5 y.orig=-2.0 min.window=-0.5 max.window=0.5 angle=90

SOLAR IW=CdZnS_CdTe_CdxTe.log min.wave=0.1 max.wave=1.5 step.wave=0.1 tonyplot CdZnS_CdTe_CdxTe.log

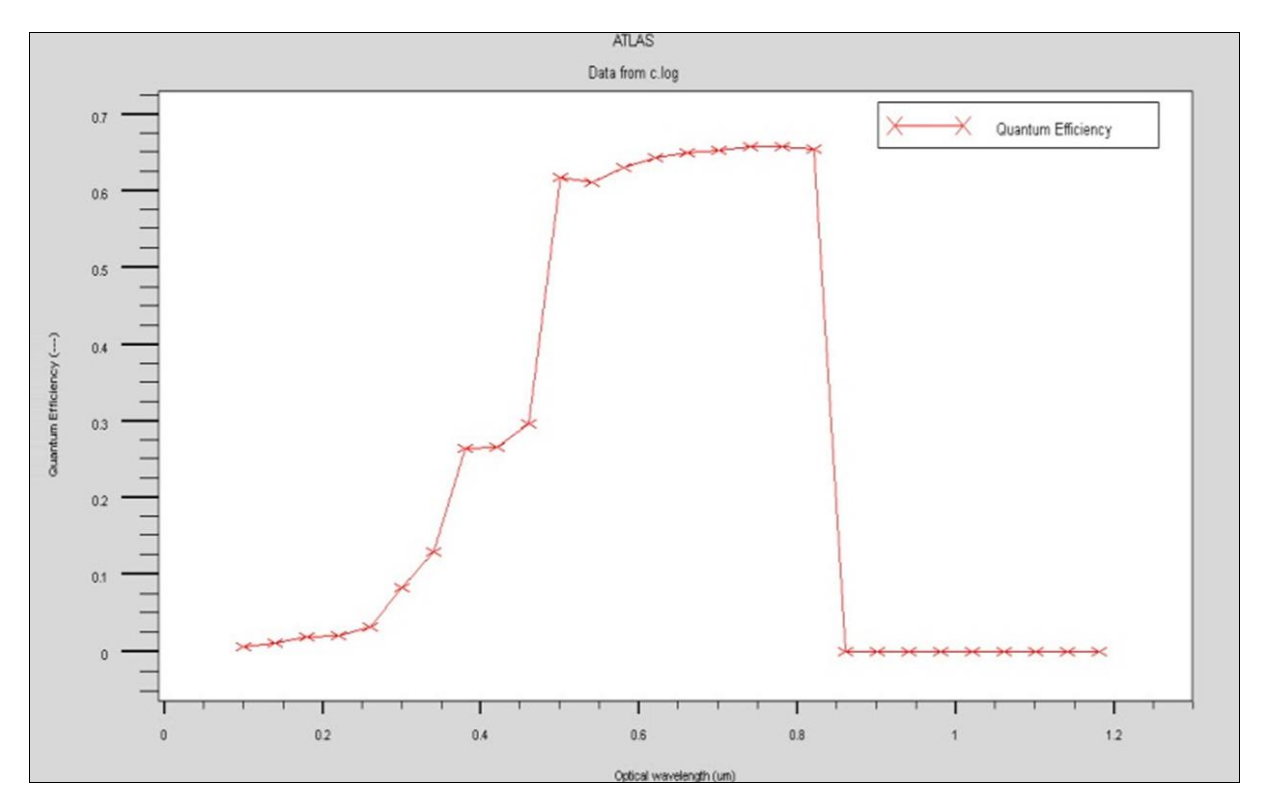


Fig 5: Spectral characteristics of CdS/CdTe solar cell simulated with S.TCAD.

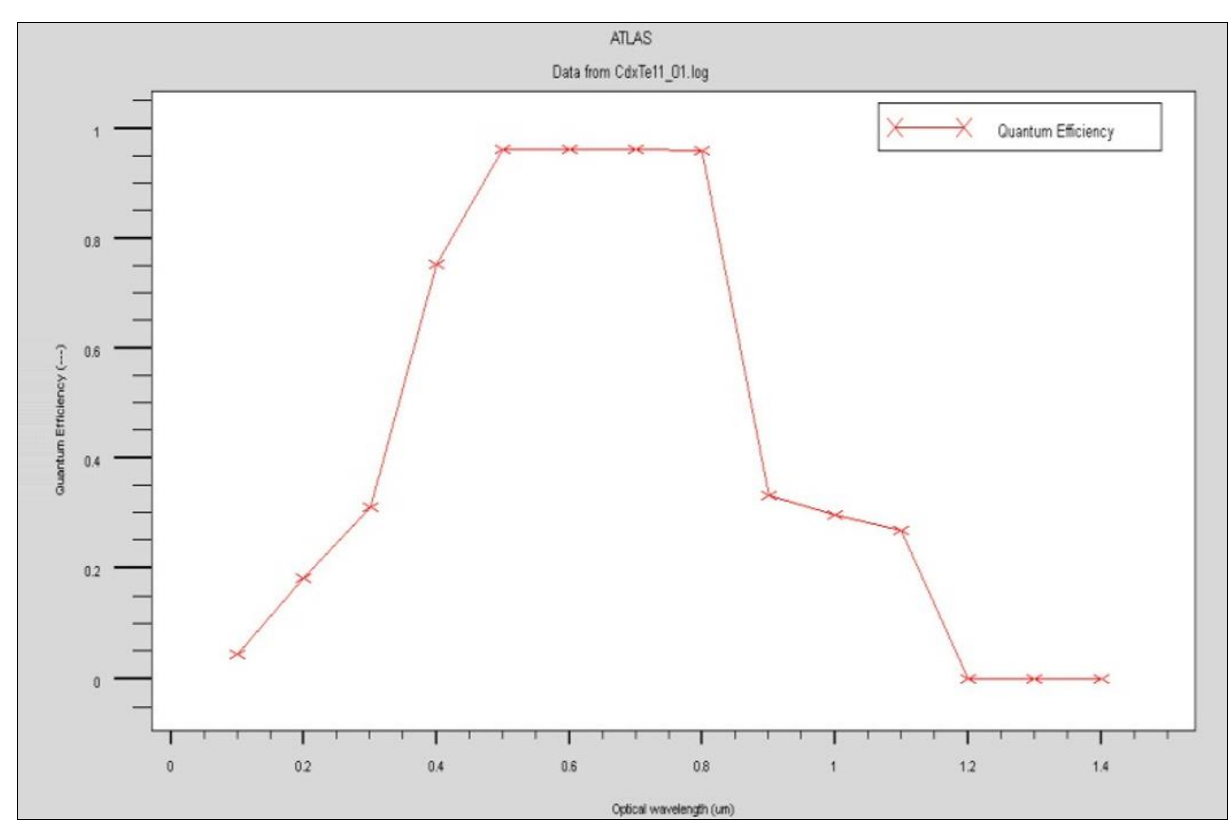


Fig 6: Spectral characteristics of Cd_{0.1}Zn_{0.9}S/CdTe/Cd_{0.2}Te solar cell simulated with S.TCAD

As shown in Fig 5 and 6, the spectral characteristics of $Cd_{0.1}Zn_{0.9}S/CdTe/Cd_{0.2}Te$ solar cell are superior to the conventional CdS/CdTe solar cell.

2.3. Determination of the optimal thickness of each layer in solar cell

To determine the optimized structure of solar cell, we

performed a simulation of the relative quantum efficiency of solar cell with the change of thickness of each layer, by varying the thickness of the Cd_{0.1}Zn_{0.9}S layer from 20 to 100 nm, the CdTe layer from 1 to 5 lm and the Cd_{0.2}Te layer from 50 to 300 nm, respectively. Fig 7, 8 and 9 show the variation of relative quantum efficiency with the thickness change of each layer, respectively.

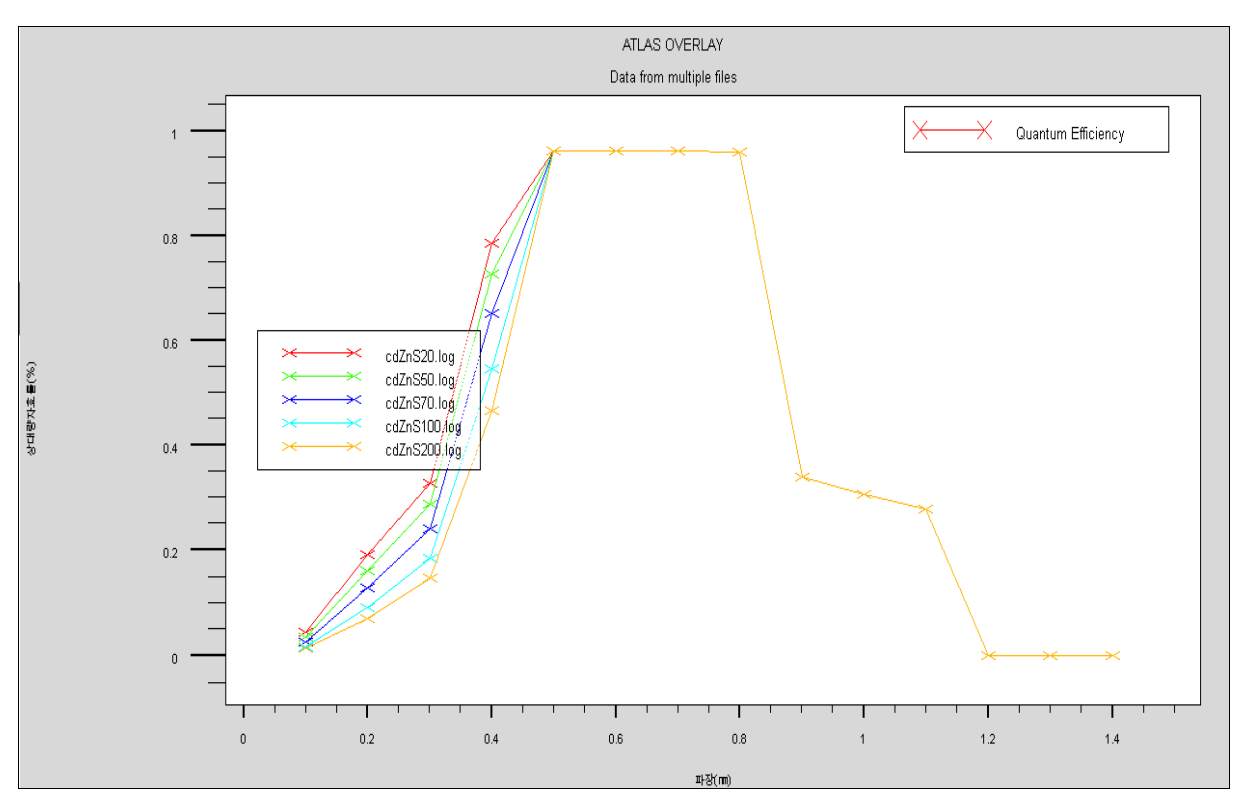


Fig 7: Relative quantum efficiency variation with thickness variation of Cd_{0.1}Zn_{0.9}S layer.

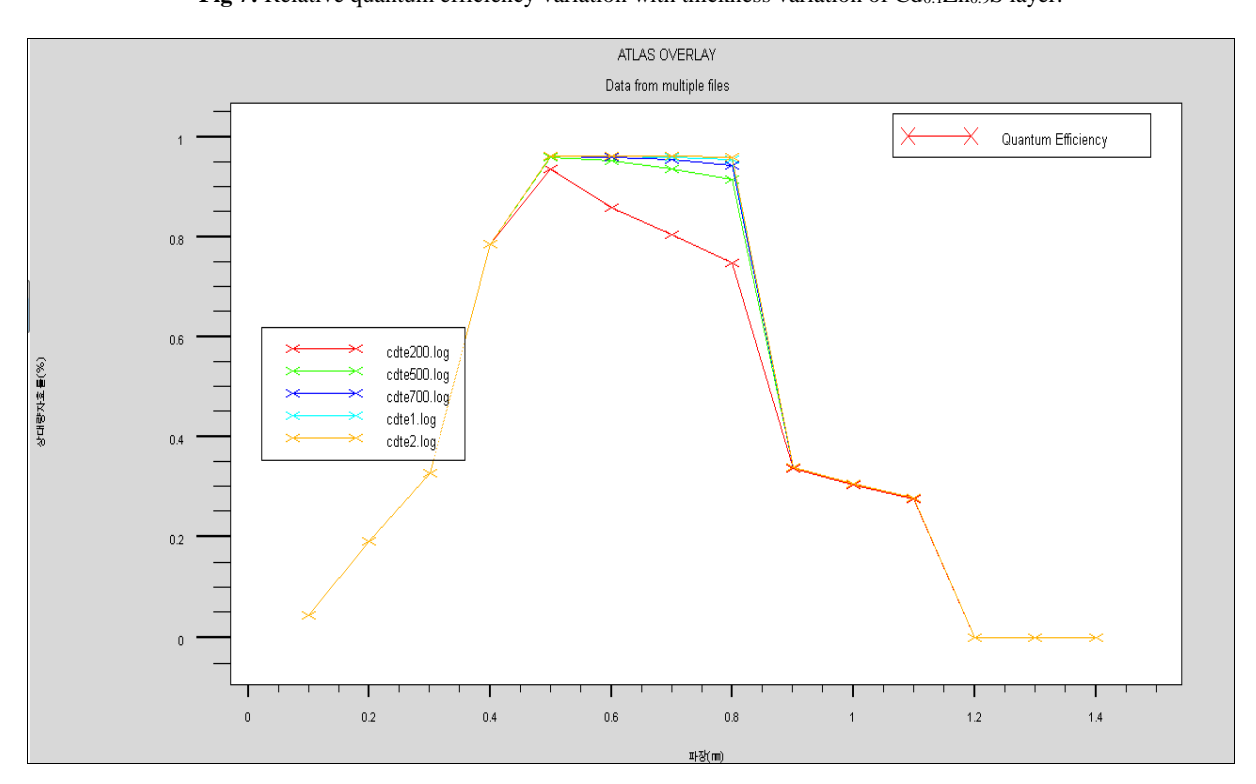


Fig 8: Relative quantum efficiency variation with thickness variation of CdTe layer

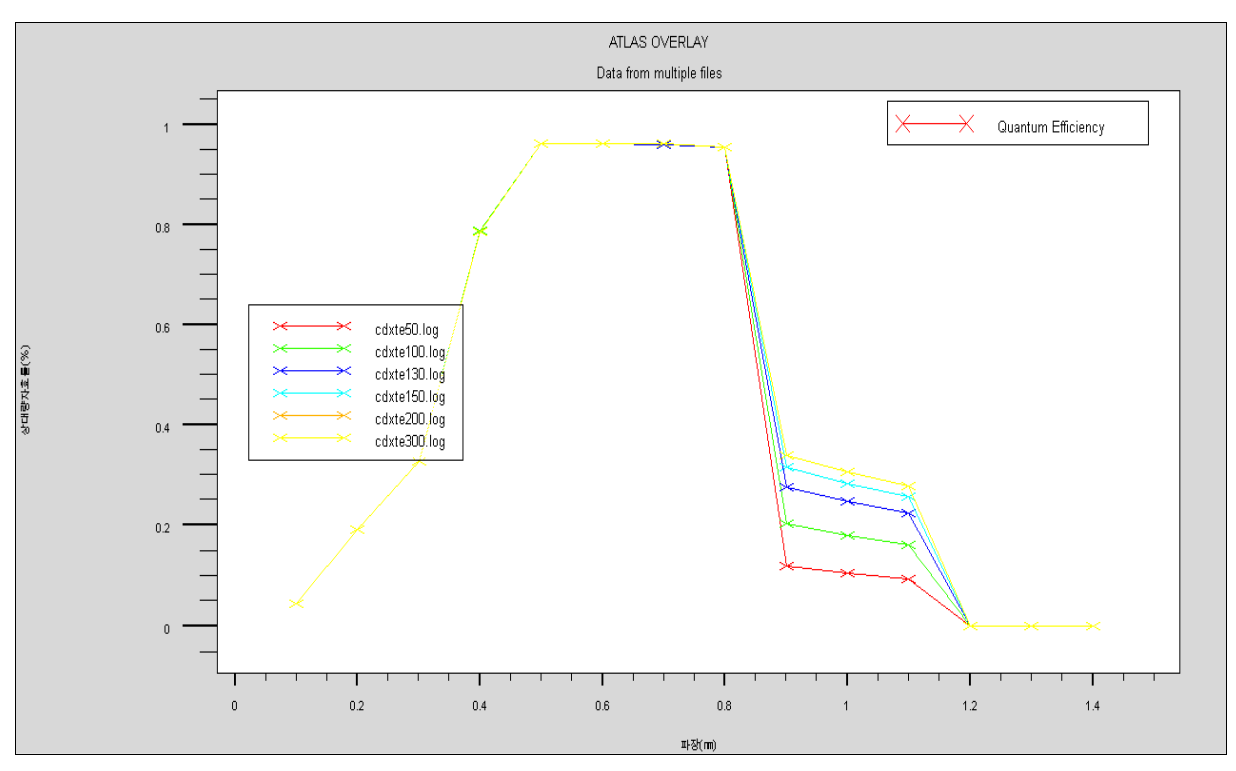


Fig 9: Relative quantum efficiency variation with Cd_{0.2}Te layer thickness variation

As shown in the figure, the thinner $Cd_{0.1}Zn_{0.9}S$ layer and the thicker the CdTe and $Cd_{0.2}Te$ layers, the higher the relative quantum efficiency of solar cell. This value are saturated at around the thickness of 1μ mCdTe and 200 nm $Cd_{0.2}Te$. Thus, the thickness of window layer should be as thin as possible, and the thickness of the absorber layer and auxiliary absorber layer can be found to be 1μ m and 200 nm, which is the best performance of solar cell.

3. Fabrication of $Cd_{0.1}Zn_{0.9}S/CdTe/Cd_{0.2}Te$ solar cells for sunshine sensor

3.1. Cd_{0.1}Zn_{0.9}S window laver fabrication

 $Cd_{0.1}Zn_{0.9}S$ polycrystalline film was deposited by Cd^{2+} , Zn^{2+} , and S^2 -ions dissolved from cadmium chloride (CdCl₂), zinc chloride (ZnCl₂), and thiourea (NH₂)₂CS [21]. The transparent conductive (SnO2:F) glass substrate was treated with 30% nitric acid solution and washed with deionized water at 60 °C. After treatment with dichromate solution at 60 °C for 1 h, it was washed three times with deionized water and then ultrasonically washed in order of ethanol and deionized water. Finally, it was washed with deionized water at 60 °C and dried. Slowly adding ammonia leads to metal complexes of free metal ions. The dissociated S²from thiourea (NH₂)₂CS reacts with the cadmium precursor Cd (NH₃)₄²⁺ and zinc precursor Zn (NH₃)₄²⁺ in aqueous ammonia to form Cd_{0.1}Zn_{0.9}S. When the ionic red [Cd²⁺] [Zn²⁺] [S²⁻] exceeds the solubility product, ions in the hydrophilic ammonia medium on the substrate start to deposit slowly into the membrane Finally, Cd_{1-x}Zn_xS films are formed on the substrate.

The reaction that occurs is as follows [21]:

$$(1-x)Cd(NH_3)_4^{2+} + xZn(NH_3)_4^{2} + S^{2-} \rightarrow Cd_{1-x}Zn_xS + 4NH_3 \uparrow$$
(10)

To prepare Cd_{0.1}Zn_{0.9}S thin films, solutions of cadmium chloride CdCl₂:1 mM, zinc chloride ZnCl₂:9 mM, thiourea

 $(NH_2)_2CS:10$ mM, ammonium chloride $NH_4Cl:20$ mM, ammonia water $NH_3H_2O:1$ M were prepared and placed in a thermostatic bath where the reaction was carried out. The substrate was mounted, the temperature was raised to 90 °C and the pH was kept at 10 by titrating ammonia water at a suitable rate. After 20 min of reaction, a uniform and dense film was deposited on the substrate. The film-coated substrate was removed, washed with deionized water and dried in a thermostatic drying oven. The thickness of the film was set to 50 nm.

3.2. Fabrication of CdTe thin film and $Cd_{0.2}$ Te auxilliary absorber layer

Cd and Te with 99.999% purity were used as the materials for the synthesis of CdTe crystals. Thus, the mass ratio of Cd to Te for the synthesis of CdTe in a 1:1 molar ratio is 0.46835:0.5316. To obtain a Cd/Te ratio of 0.2, weigh Cd and Te to 0.2:1 molar ratio and 1:5.67 mass ratio, respectively. Add the weighed Cd and Te to the quartz glass tube and heat at 820 °C to form a lump with a mixture of Cd and Te of 0.2.

The synthesized bulk $Cd_{0.2}Te$ was ground and mixed with high purity alcohol to make a paste and spread on a photographic plate glass. Put it in the proximity sublimation unit, gradually raise the temperature of the source substrate to 300 °C, vacuum evacuate the impurities contained in the substrate and source, and raise the source temperature to 520 °C to start sublimation. The substrate temperature was kept at 300 °C and oxygen and argon gas were injected. After sublimation, the exhaust is removed again and the temperature is gradually lowered to take out the sample at around 50°C. Then, the samples were heat treated at 185 °C in nitrogen gas.

3.3. Back-electrode formation

The back electrode was formed by evaporating Ag. Molybdenum sheet was cut into required size and etched in dilute nitric acid slowly to 0.1~0.15 mm thick before

making a boat. The coatings were carried out at a pressure of 10⁻² Torr and a temperature of 1047 °C. After

evaporation, it is waited for 5 minutes before taking out the sample.

4. Analysis of the characteristics and defect detection of the sunshine sensor.

4.1. Characterization of solar cells for sunshine sensor applications

The current-voltage characteristics of solar cells were measured by the variable resistance method. The measured results are shown in Fig. 10. The short-circuit current and open-circuit voltage of the solar cell were 20.8 mA and 0.7 V, respectively.

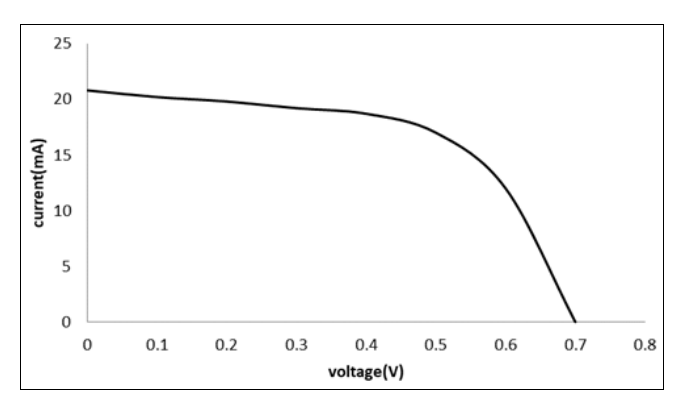


Fig 10: Current-voltage characteristics of solar cells

The current values with radiation intensity were measured using a multifunction meter UT203 using 220 V-1000 W halogen lamp, which can simulate solar radiation as a source. Different irradiance intensities were obtained by

varying the distance between the light source and solar cell. The current and radiation intensity dependence obtained by this method is shown in Fig. 11.

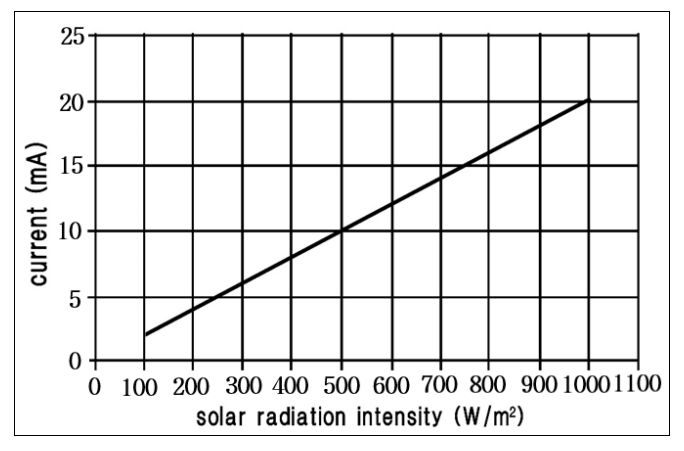
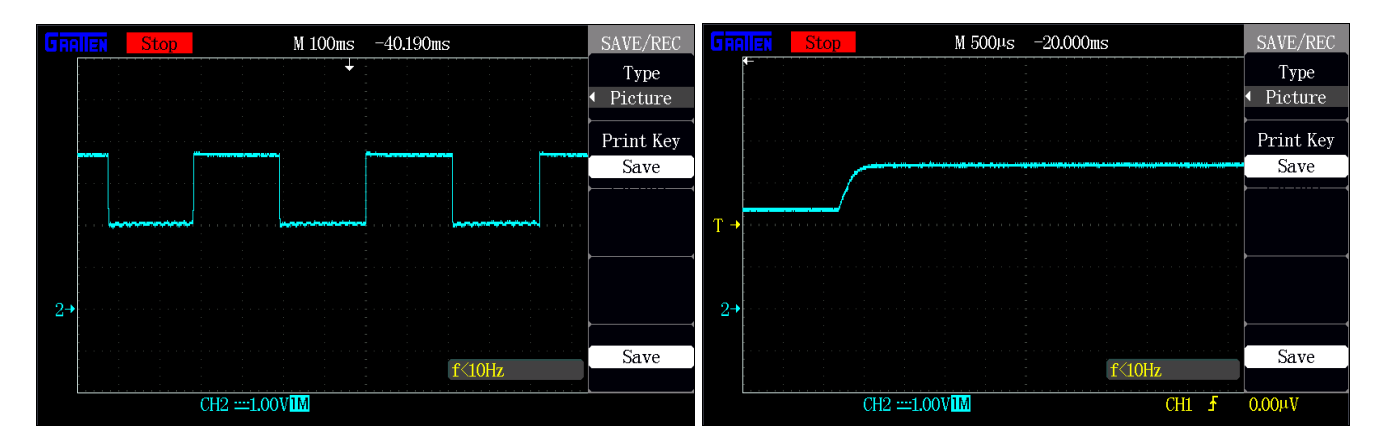


Fig 11: Relationship between current of solar cell and radiation intensity

As shown in figure, the current increased linearly when the irradiance of simulated light source was varied from 100 to 1000 W/m^2 . After a halogen lamp with a radiation intensity of 400 W/m^2 , the open circuit voltage of solar cell was measured with a GA1202 CAL oscillometer, with the

halogen lamp switch on and off at 1 s intervals. The measured rise and fall times of the fabricated solar cells were $250\mu s$ and $500\mu s$, respectively. The measurement results are shown in Fig. 12.



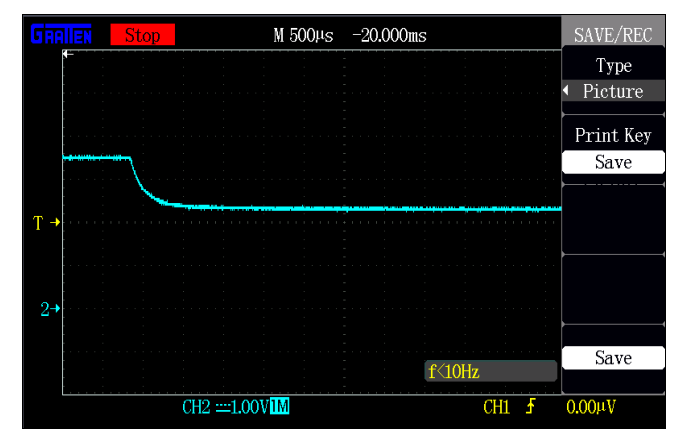


Fig 12: Response characteristics, rise time and fall time

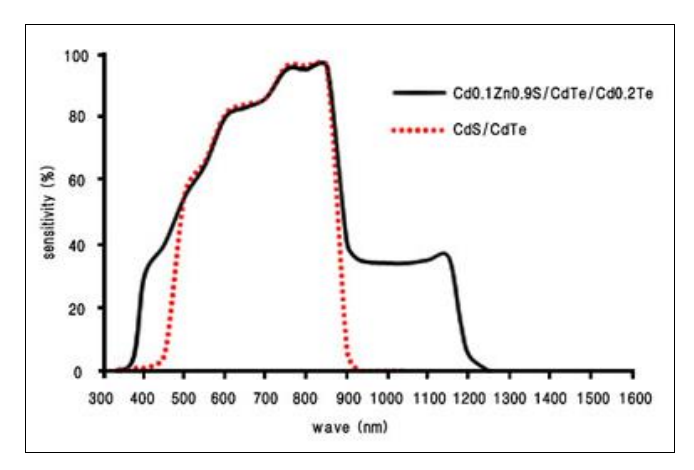


Fig 13: Spectral characteristics

The spectral characteristics were measured using a spectrophotometer. From the figure 13, it can be seen that the spectral response of fabricated solar cell is wider than that of the conventional solar cell, and the range is between 400 and 1200 nm.

4.2. Fault inspection: Thin film solar cells exhibit various defects, including shunt defects, corrosion and cracking due to impurities, micro-crack, scratches, etc., during fabrication and characterization. Particularly, the thin film often causes shunt defects, which are invisible and have a negative effect

on the solar cell properties, and should be examined. Electroluminescence (EL) technology has been widely used for the detection of solar cells due to its advantages of simplicity, speed, and non-destructive operation [22-24].

In the defective part, the light intensity is different from the defect-free part, and hence the defect part can be easily detected. The emitted light intensity is affected by forward bias voltage and current. Therefore, the test setup was fabricated and tested on the solar cell. The configuration and test principle diagram of the test device manufactured are shown in Figs. 14 and 15.

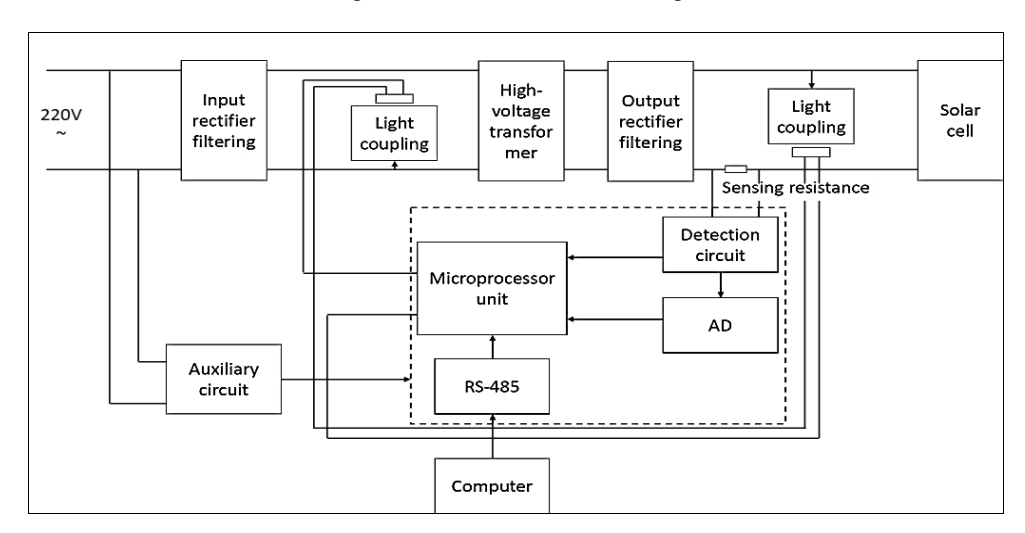


Fig 14: Configuration of test set

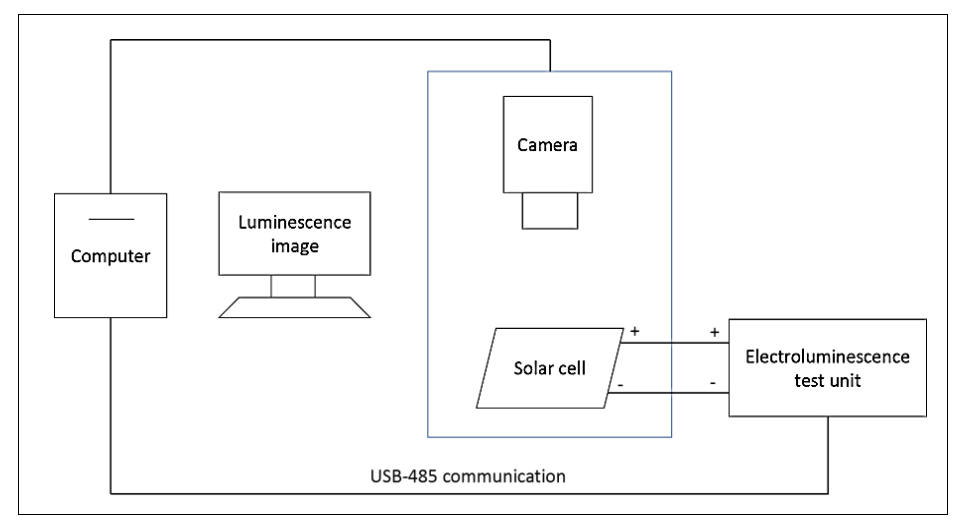


Fig 15: Test block diagram

The previously prepared solar cells were tested using the fabricated device. The voltage is set to the open circuit voltage of the solar cell and the duty ratio is adjusted to increase the output current by 5 mA, up to the short circuit

current of the solar cell. The camera is mounted on the solar cell chip and the images are captured by a computer. The acquired image is shown in Fig. 16.

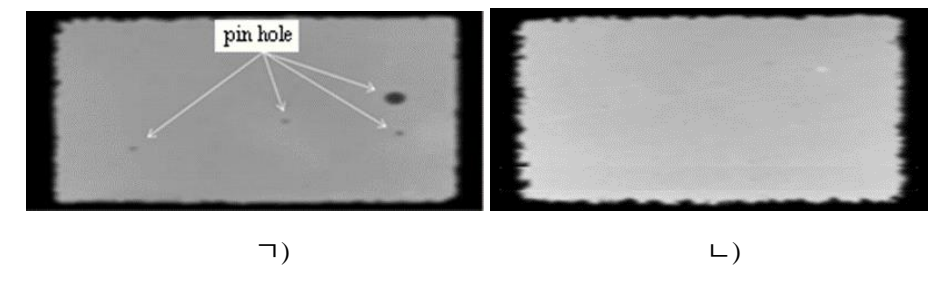


Fig 16: Test image (a defective solar cell, b normal solar cell)

Among the solar cells fabricated, the solar cell with shunt defect is not used for sunshine sensor fabrication.

5. Design, fabrication and characterization of sunshine sensor:

- 5.1. Design and fabrication of sensors
- 5.1.1 Structural Design of Sensors

To rationally determine the structure of sunshine sensor, it need to know the apparent trajectory of the sun's motion. The earth rotates with an axis inclined at an angle of 23.5° and not about an axis perpendicular to the plane that orbits the sun. The observed apparent trajectory of the sun is shown in Fig. 17 below.

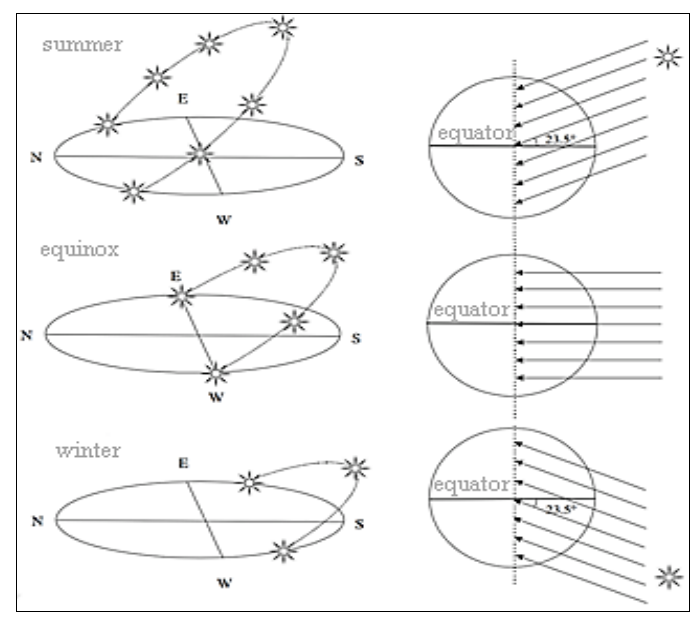


Fig 17: Apparent trajectory of the sun motion

The angle of incidence of sunlight varies with latitude and season. During a day, the sun travels at 15° intervals in one hour, so that the angle of incidence varies with time [9-13]. Considering the motion of sun, a groove for installing solar cells in sunshine sensor is determined and placed in a circular shape. The number of solar cells in the sensor was 16 because the sun moved to 15° in 1 h, and the slot size for the solar cell was $3 \text{ mm} \times 25 \text{ mm}$.

Next, an angle dial is designed to set the sensor angle with respect to latitude. To observe the sun with a simple circular motion using the equatorial coordinate system, the axis of rotation was aligned with the axis of the celestial axis. In other words, the dial is aligned with the equatorial plane at an angle of the vertical direction and the latitude of the observation point, perpendicular to the axis of rotation. The high latitude at the station lowers the altitude of the sun, and the low latitude at the station raises the altitude of the sun. The appearance of the fabricated sunshine sensor is shown in Fig. 18.



Fig 18: Appearance of the sunshine sensor

5.1.2. Circuit design of the sensor

In solar cells, the response to sunlight is represented by the open circuit voltage and short circuit current. To measure sunshine time with solar cells, we used the short-circuit current of solar cell. The reason is that the relationship between the short-circuit current and solar radiation intensity of solar cells is as following.

$$I=I_0\times[1+K_I(T-T_0)]G/G_0$$
 (11)

- **I**₀: short-circuit current of solar cell under normal conditions (1000 W/m², 25 °C).
- K_I: short-circuit current gain coefficient of solar cell (%/C)
- T₀: temperature under standard conditions (25°C)
- G₀: radiation intensity under standard conditions (1000 W/m²)

Deriving the solar radiation intensity from Eq. 11:

$$G = \frac{IG_0}{I_0 \times [1 + K_I (T - T_0)]}$$
 (12)

Also, the sunshine sensor should detect the short-circuit current and temperature of solar cell from Eq. 12, since the solar radiation should be more than 120 W/m² or not. The short-circuit current of the fabricated solar cell of size 0.75 cm² is 15 mA under normal conditions. And the temperature sensor DS18B20 was used to sense the temperature of solar cell. The DS18B20 temperature sensor has 9-12 bits of resolution, it has a range of operating voltages and temperatures of 3-5 V, 55°C -125°C, respectively. The measurement accuracy is ± 0.5 °C at -10°C- 80°C. Since the current produced by solar cell is small, the current was converted into voltage using a current-voltage converter circuit.

The current-voltage converter circuit is shown in Fig. 19.

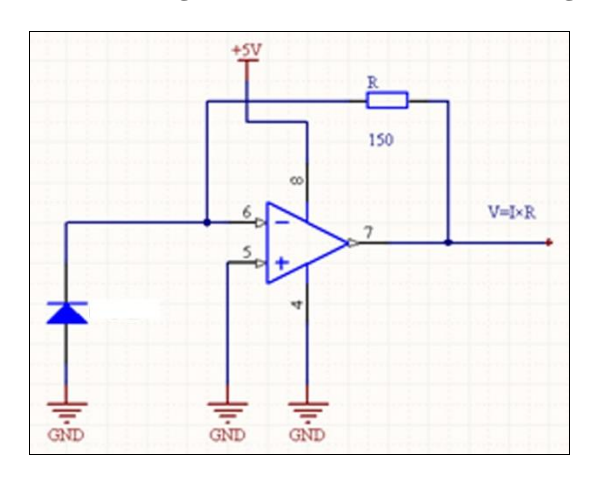


Fig 19: Current-voltage converter circuit

The output voltage relationship is expressed as following.

$$V=I\times R \tag{13}$$

Where I is the short-circuit current of solar cell, and R is the negative feedback resistance for the current gain. Since the short-circuit current of solar cell is 20 mA when solar radiation is $1000~W/m^2$, a negative feedback resistance of 100Ω is used to ensure maximum voltage not exceeding 3 V. The temperature measurement circuit using the temperature sensor DS18B20 is shown in Fig. 20 below.

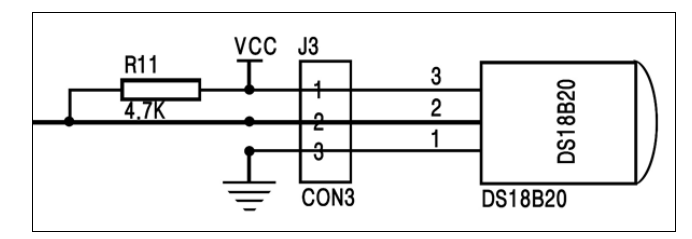


Fig 20: Temperature sensing circuit

The output of the current-voltage converter circuit and the temperature sensor circuit were connected to the A/D port of the microcomputer. The algorithm for measuring the sunshine time is shown in Fig. 21.

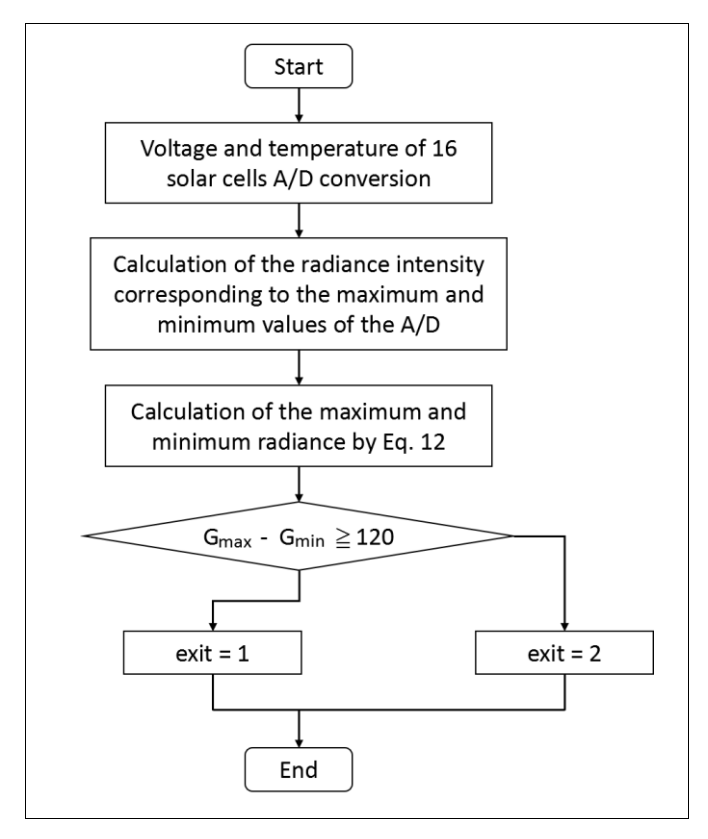


Fig 21: Sensor measurement algorithm

5.2. Sensor characterization

A comparative characterization analysis between the CSD3-group sensor and fabricated sensor using photodiode was

carried out. The output signal changes of sensor during the day are shown in Figs. 22, 23 and 24.

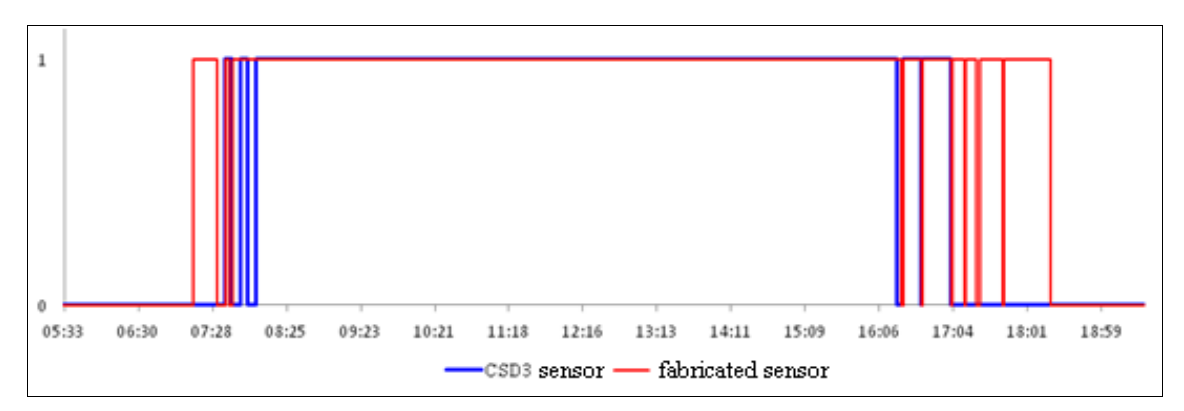


Fig 22: Output signal variation process of sensors during a day

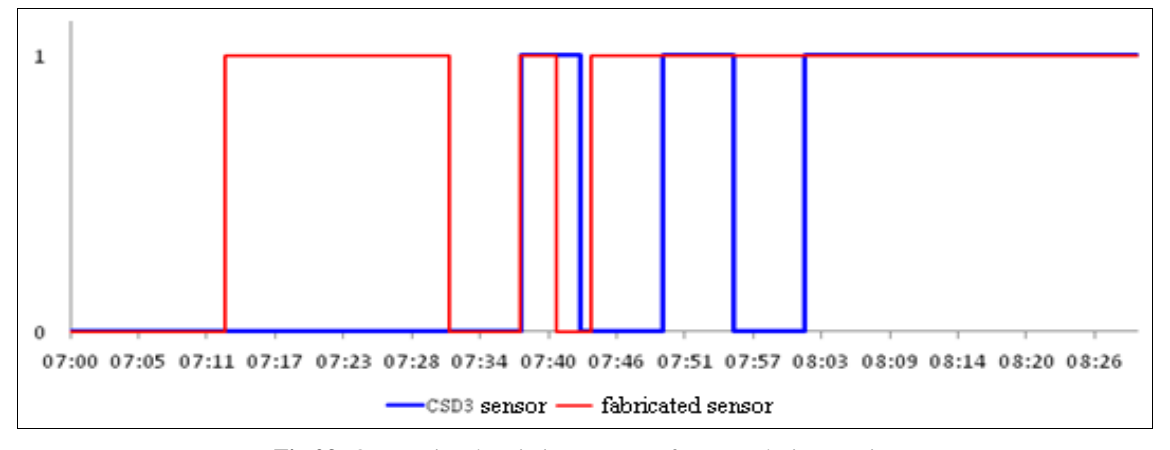


Fig 23: Output signal variation process of sensors during sunrise

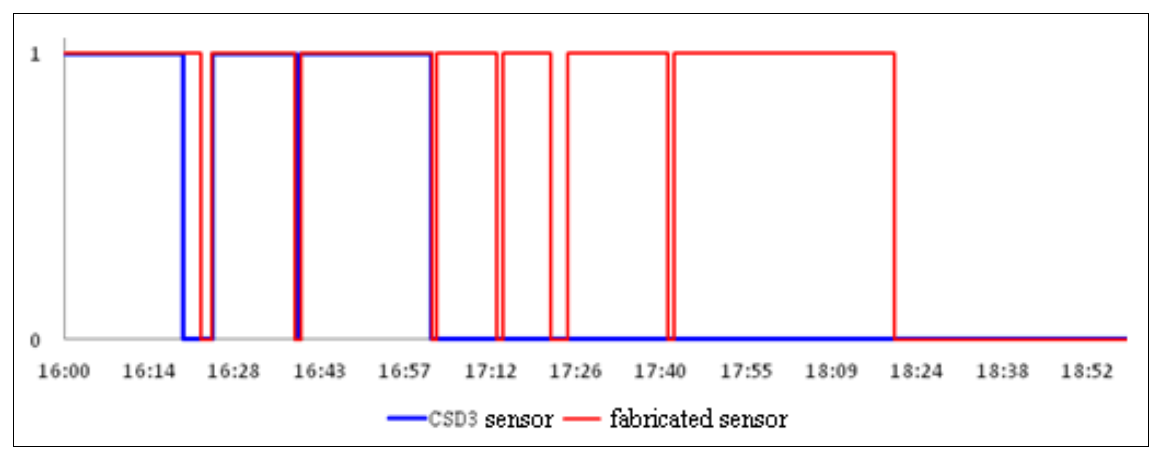


Fig 24: Output signal variation process of sensors during sunset

Table 2: Output signal variation of sensors during the day

Fa	bricated sensor	C	SD3 sensor	fabr	icated sensor	C	CSD3 sensor
Time	Output signal level						
05:20	0	05:20	0	17:02	1	16:25	1
07:13	0	07:13	0	17:02	0	16:39	1
07:13	1	07:13	0	17:03	0	16:39	0
07:32	1	07:32	0	17:03	1	16:40	0
07:32	0	07:32	0	17:13	1	16:40	1
07:38	0	07:38	0	17:13	0	17:02	1
07:38	1	07:38	1	17:14	0	17:02	0
07:41	1	07:43	1	17:14	1	17:14	0
07:41	0	07:43	0	17:22	1	17:22	0
07:44	0	07:50	0	17:22	0	17:22	0
07:44	1	07:50	1	17:25	0	17:25	0
16:23	1	07:56	1	17:25	1	17:25	0
16:23	0	07:56	0	17:42	1	17:42	0
16:25	0	08:02	0	17:42	0	17:42	0
16:25	1	08:02	1	17:43	0	17:43	0
16:39	1	16:20	1	17:43	1	17:43	0
16:39	0	16:20	0	18:20	1	18:20	0
16:40	0	16:23	0	18:20	0	18:20	0
16:40	1	16:25	0	19:33	0	19:33	0

As can be seen in the above figures and tables, the fabricated sensor reacts 25 minutes faster at sunrise and 41 minutes later at sunset than the CSD3 sensor. Thus, the time difference of the output signal change between the fabricated sensor and the CSD3 sensor is about 1 h, which is superior to the fabricated sensor. The characteristics of the fabricated sensor and CSD3 sensor are shown in Table 3.

Table 3: Characteristics of the sunshine sensor

No	Index	Fabricated sensor	CSD3 sensor
1	wavelength band	400~1200nm	400~1100
2	measurement accuracy	95%~	90%
3	response time	0.5	1s
4	threshold value	120W/m²±10%	120 W/m²±20%
5	power	5V	12V

Conclusions

The contributions of this paper are as follows.

First, in order to fabricate the sunshine sensor using solar cell, we established a CdTe solar cell simulation system and selected the optimal thickness of solar cell. Simulations of CdTe solar cells with the auxiliary absorber layers were performed using the S.TCAD semiconductor device simulation tool to determine the spectral band broadening and the optimum thickness of each layer for solar cell

fabrication.

Second, CdTe solar cells with additional absorber layers were fabricated and tested. The fabrication process of transparent conductive layer, window layer, absorber layer and auxiliary absorber layer was established, the current-voltage characteristics, spectral response characteristics of solar cell were analyzed, and the solar cell was tested for use in the fabrication of the sensor using an electroluminescence test device.

Third, the design of the structure and circuit of the sunshine sensor was carried out and the characteristics of sensor were compared and analyzed. The fabricated sensor was compared with the CSD3 sensor to confirm its superior performance. The sensor is simple in principle, low in cost and can be used for meteorological observation and agricultural production as well as for the development of solar energy.

Acknowledgment

This work was supported by Kim Chaek University of Technology, Democratic People's Republic of Korea. The supports are gratefully acknowledged. The authors express their gratitude to the editors and the reviewers for their helpful suggestions for improvement of this paper.

Funding: This research did not receive the external funding.

References

- 1. da Rocha ÁB. Development and validation of an autonomous system for measurement of sunshine duration. Sensors. 2020;20:4606:1-12.
- 2. Matuszko D. A comparison of sunshine duration records from the Campbell-Stokes sunshine recorder and CSD3 sunshine duration sensor. Theoretical and Applied Climatology. 2014;119:401-406.
- Hong C. Development of a light-heat electrical measurement sunshine recorder. PLA University of Science and Technology. 95019.
- 4. Breniuc L, Haba C. A development system for sunshine duration estimation. Electrotehnică, Energetică, Electronică. 2013;4:79-91.
- 5. Rocha A, Diniz J. Development and test of an electronic sunshine duration recorder. COBEM. 2019;25:10-18.
- 6. Muneer T, Zhang X, Wood J. Evaluation of an innovative sensor for measuring global and diffuse irradiance and sunshine duration. International Journal of Solar Energy. 2014;22:115-122.
- 7. Li YJ. The effect of different preparation temperatures on the photoelectric properties of *CdTe* films and solar cells. Acta Physica Sinica. 2010;59(1):625-629.
- 8. Morales-Acevedo A. Thin film *CdS/CdTe* solar cells: Research perspectives. Solar Energy. 2006;80:675-681.
- 9. Bernal-Condia A. Simulation of a thin-film solar cell based on kesterite using MATLAB. Journal of Physics: Conference Series. 2019;1159:012020:1-7.
- 10. Thahab SM, *et al*. The optical properties of $Cd_{1-x}Zn_xS$ thin films on glass substrate prepared by spray pyrolysis method. Optik. 2014;125:5112-5115.
- 11. Kartopu G, *et al*. Effect of window layer composition in $Cd_{1-x}Zn_xS/CdTe$ solar cells. Progress in Photovoltaics: Research and Applications. 2014;22:18-23.
- 12. Rojas JA. A double energy transition of nanocrystalline $Cd_{1-x}Zn_xS$ films deposited by chemical bath. Materials and Manufacturing Processes. 2015;30:785-792.
- 13. Tian C, *et al.* $Cd_{1-x}Zn_xS$ thin films with low Zn content prepared by chemical bath deposition. International Journal of Photoenergy. 2012;1-5.
- 14. Carreón-Moncada I, *et al.* $Cd_{1-x}Zn_xS$ thin films with low Zn content obtained by an ammonia-free chemical bath deposition process. Thin Solid Films. 2013;548:270-274.
- 15. McCandless BE, Dobson KD. Processing options for *CdTe* thin film solar cells. Solar Energy. 2004;77(6):839-856.
- 16. Parameshwari PM, Naik GK. Spray deposition and characterization of nanocrystalline $Cd_{1-x}Zn_xS$ thin films. International Journal of Nanotechnology and Applications. 2017;11(1):45-58.
- 17. Xu X. Study on influences of *CdZnS* buffer layer on *CdTe* solar cells. Superlattices and Microstructures. 2017;1016:1-8.
- 18. Ameen M. A computational study on energy bandgap engineering in performance enhancement of *CdTe* thin film solar cells. Results in Physics. 2017;7:1066-1072.
- 19. Rousset J. Structure and optoelectronics of electrodeposited cadmium ditelluride (*CdTe*₂). Chemistry of Materials. 2008;20:6550-6555.
- 20. Maiti CK. Introducing technology computer-aided

- design (TCAD): Fundamentals, simulations, and applications. Singapore: Pan Stanford Publishing Pte. Ltd.; 2017. p. 1-25.
- 21. Goudon T. On the Shockley-Read-Hall model: Generation-recombination in semiconductors. SIAM Journal on Applied Mathematics. 2007;67(4):1183-1201
- 22. Hun KD. Investigation on the influence of Zn content on the structural, optical, morphological, and electrical properties of ternary compound $Cd_{1-x}Zn_xS$ window layer for CdTe solar cell. Functional Materials Letters. 2023;16(8).
- 23. Dhimish M. Ultra-fast high-resolution solar cell cracks detection process. IEEE Transactions on Industrial Informatics. 2019;1-8. doi:10.1109/TII.2019.2946210.
- 24. Demant M. Microcracks in silicon wafers II: Implications on solar cell characteristics, statistics and physical origin. IEEE Journal of Photovoltaics. 2016;6(1):136-144.
- 25. Zumbo L. Influence of defects on silicon heterojunction solar cell efficiency: Physical model and comparison with data. AIP Advances. 2021;11:015044.